

Heterostrain Determines Flat Bands in Magic-Angle Twisted Graphene Layers

Florie Mesple,^{1,*} Ahmed Missaoui,² Tommaso Cea,^{3,4} Loic Huder,⁵ Francisco Guinea,^{3,6}

Guy Trambly de Laissardière², Claude Chapelier,¹ and Vincent T. Renard^{1,†}

¹Université Grenoble Alpes, CEA, Grenoble INP, IRIG, PHELIQS, 38000 Grenoble, France

²Laboratoire de Physique Théorique et Modélisation (UMR 8089), CY Cergy Paris Université, CNRS, 95302 Cergy-Pontoise, France

³Imdea Nanoscience, Faraday 9, 28015 Madrid, Spain

⁴Instituto de Ciencia de Materiales de Madrid, CSIC, Sor Juana Inés de la Cruz 3, Cantoblanco, 28049 Madrid, Spain

⁵European Synchrotron Radiation Facility (ESRF), 71 Avenue des Martyrs, 38000 Grenoble, France

⁶Donostia International Physics Center, Paseo Manuel de Lardizábal 4, 20018 San Sebastián, Spain



(Received 5 January 2021; accepted 29 July 2021; published 17 September 2021)

The moiré of twisted graphene bilayers can generate flat bands in which charge carriers do not possess enough kinetic energy to escape Coulomb interactions with each other, leading to the formation of novel strongly correlated electronic states. This exceptionally rich physics relies on the precise arrangement between the layers. Here, we survey published scanning tunneling microscope measurements to prove that near the magic-angle, native heterostrain, the relative deformations between the layers, dominates twist in determining the flat bands as opposed to the common belief. This is demonstrated at full filling where electronic correlations have a weak effect and where we also show that tip-induced strain can have a strong influence. In the opposite situation of zero doping, we find that electronic correlation further renormalizes the flat bands in a way that strongly depends on experimental details.

DOI: [10.1103/PhysRevLett.127.126405](https://doi.org/10.1103/PhysRevLett.127.126405)

The strongly correlated electron physics recently observed in twisted graphene layers [1,2] develops in flat bands [3,4], which are very sensitive to the relative arrangement between the layers. For instance, the superconducting phase has been reported to occur in a very narrow range of rotation angle between the layers around the magic angle. As another illustration, hydrostatic pressure changes the interlayer distance, which also strongly influences superconductivity [5,6]. Heterostrain, the in-plane deformation of one layer with respect to the other, is an ubiquitous source of modification of the relative arrangement between the layers [7–16]. Experiments [7] and theory [17,18] have shown that heterostrain affects the flat bands, which could have an impact on the strongly correlated electron physics. Bi *et al.* have even predicted that near the magic angle, the bandwidth becomes *insensitive* to the twist angle and that the effect of heterostrain is *dominant* [18], calling for systematic experimental study of its effect. Such program is, however, difficult to implement owing to the lack of controllability of heterostrain and its inhomogeneity, sometimes referred to as “twist angle disorder” and which was also found to impact strongly correlated states at the macroscopic scale [14,19]. In order to overcome these issues, we survey already published experimental scanning tunneling microscope (STM) data [7–15] in view of quantifying the effect of homogeneous heterostrain on the physics of magic-angle twisted graphene layers.

Figure 1 presents typical STM images collected from Refs. [7–9] (see Supplemental Material for further

information [20]). An immediate observation is that the STM images all look very similar. This is not surprising because these samples have a twist angle (θ_{int}) very close to one another. This similarity is only apparent as evidenced by the variety of shapes of the local density of states (LDOS) measured from the $dI/dV(V)$ spectroscopy [Fig. 1(d)]. Despite the fact that the flat bands should merge at the magic angle, the spectra of Refs. [8,9] show two van Hove singularities, indicating that the flat bands are still separated. Their spacing ΔE_{exp} is doping dependent, which has been attributed to electron-electron interactions [8–13]. It can reach several tens of meV, even at large doping where correlations are not expected to renormalize strongly the bands. Still, while the two samples have a twist angle differing by only 0.1° , doping does not explain why their ΔE_{exp} differ by a factor of 2–3. Sample to sample variation is obvious from other published data [10–15]. Strikingly, the data of Ref. [7] show a third peak at zero energy, a result that was recently reproduced [16]. In order to determine whether this variety in sample behavior can be understood within the framework of heterostrain, we use the method described in Ref. [27] to determine the precise arrangement of the layers and calculate the corresponding local density of states using a tight-binding method [3,28,29].

Figures 1(a)–1(c) include our estimates of heterostrain. In all cases, biaxial heterostrain (ϵ_{bi}) is smaller than uniaxial heterostrain (ϵ_{uni}), which varies by a factor of 3 from the smallest to the largest. Figure 1(e) shows that the calculated local density of states agrees very well with

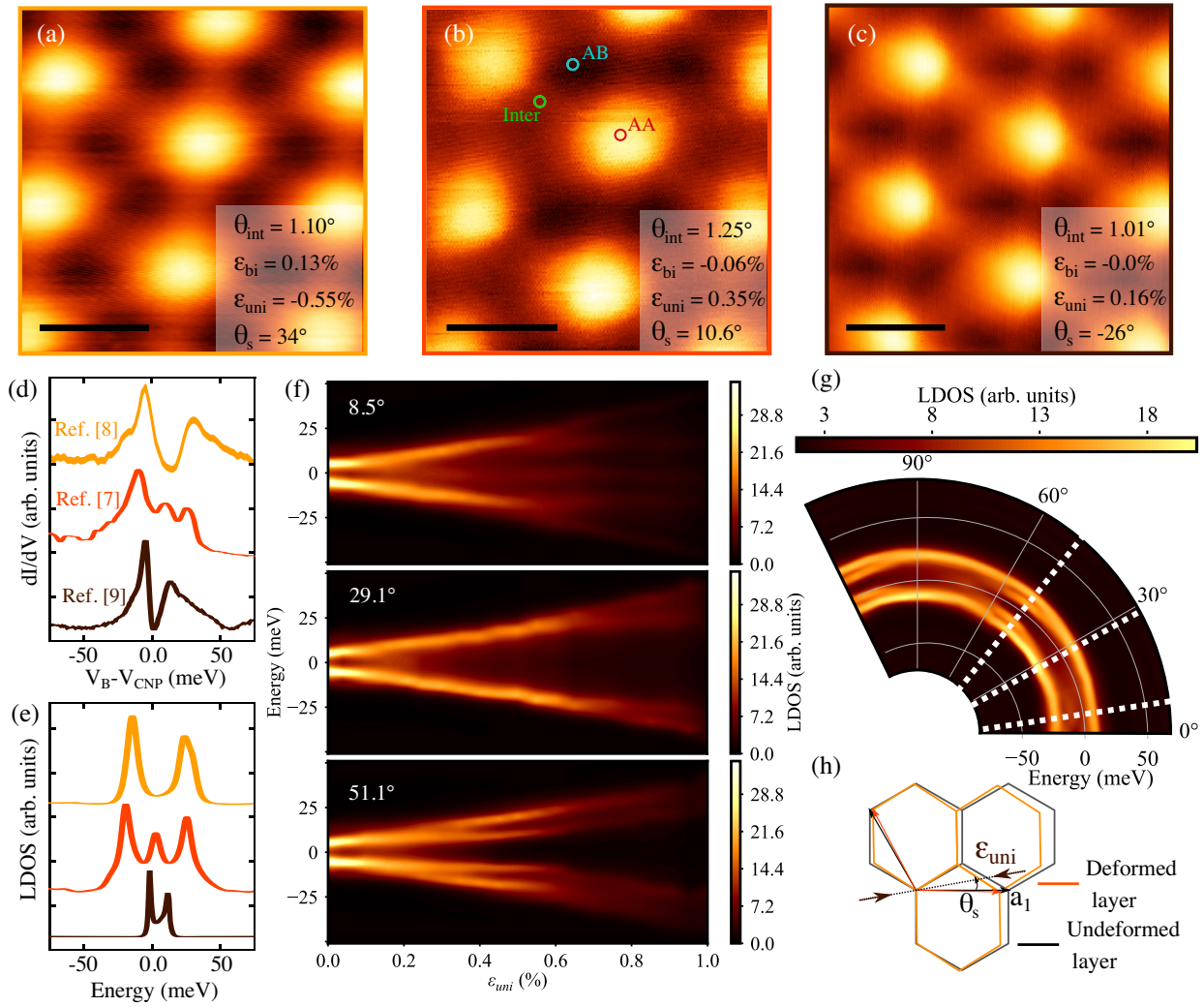


FIG. 1. Heterostrained twisted graphene layers. (a)–(c) STM images of twisted graphene layers near the magic angle adapted from (a) Refs. [8], (b) [7], and (c) [9], respectively. The scale bar is 10 nm in each image. Topographies were taken at 0.5 V and 30 pA, 0.4 V and 50 pA, and 0.5 V and 50 pA, respectively. Insets present the parameters describing the relative arrangement of the layers in good agreement with estimates of the original studies [7–9]. (d) Local density of states measured in the AA regions for each of the samples of (a)–(c). (e) Corresponding tight-binding calculation of the LDOS including heterostrain. (f) Tight-binding prediction for the local density of states in AA regions as function of energy and for increasing uniaxial heterostrain. The variations are plotted for three different angles θ_s of application of heterostrain. (g) Local density of states calculated for 0.4% of heterostrain applying along varying θ_s . The white dotted lines indicate the values of angles used in (f). (h) Sketch of uniaxial heterostrain configuration. One layer is deformed by a uniaxial heterostrain applied along the direction defined by θ_s and then rotated by an angle θ with respect to the undeformed layer.

experimental data. In particular, the number of peaks is controlled by heterostrain, which also influences their spacing, pointing to a strong contribution of heterostrain to the observed phenomenology. The tight-binding calculations presented in Fig. 1(f) show that the van Hove singularities separate linearly with uniaxial heterostrain for all angle θ_s of application of heterostrain. This angle controls the splitting of the van Hove singularities [Fig. 1(g)], leading to three typical behaviors reported in Fig. 1(f). Figure 1(g) shows that the density of states interpolates between these behaviors for other θ_s (see Supplemental Material and videos for more theoretical results [20]). These results agree with those of the

continuum model [18]. The more quantitative comparison of Fig. 2(a) shows that ΔE_{exp} converges to the value ΔE_{TB} predicted by our tight-binding calculation at the full doping of the flat bands. This has to be expected because the effect of electronic correlations measured by the ratio of Coulomb to kinetic energy reduces with doping and the system evolves toward the noninteracting situation modeled by our tight-binding calculations. It establishes that heterostrain controls the physics of twisted graphene layers near the magic angle at such large doping. This can be viewed explicitly in Fig. 2(b), which shows that ΔE_{exp}^0 , the experimental spacings of van Hove singularities at full filling, depends linearly on heterostrain as predicted by

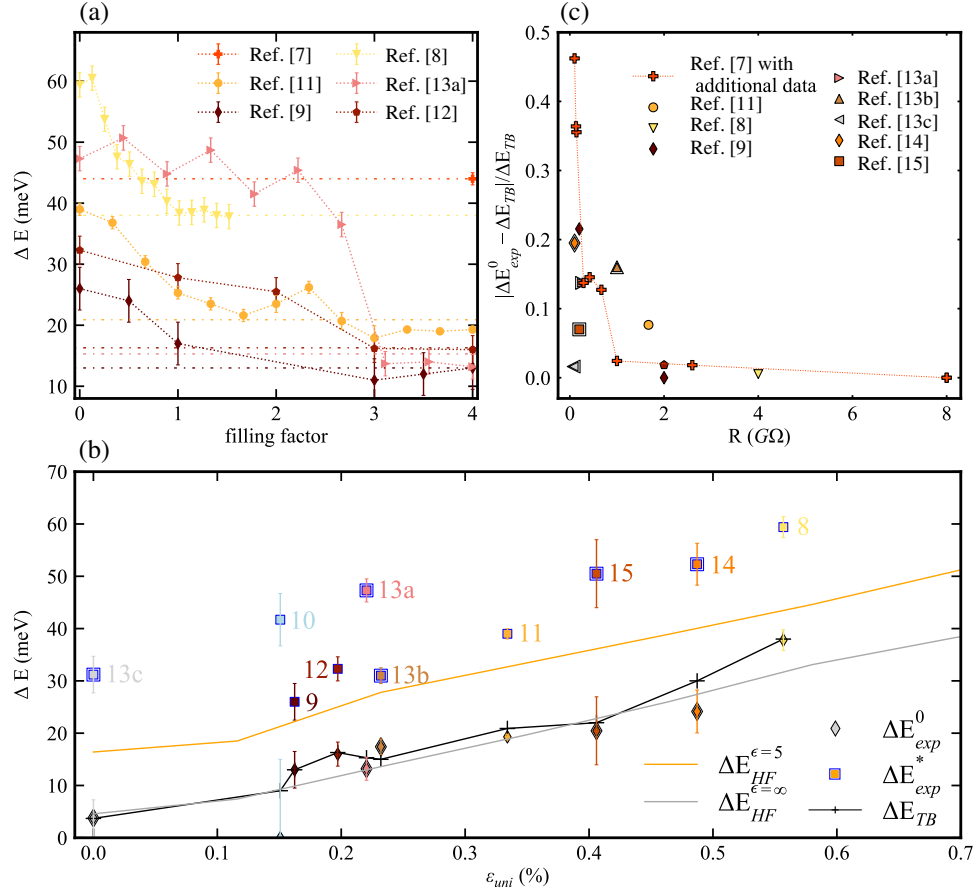


FIG. 2. Comparison between theory and experiments. (a) Representative doping dependence of the spacing between van Hove singularities. The horizontal line corresponds to prediction by tight-binding calculations with heterostrain. (b) Experimental spacing of van Hove singularities at large doping (ΔE_{exp}^0), zero doping (ΔE_{exp}^*), theoretical tight binding (ΔE_{TB}), low-interaction Hartree-Fock ($\Delta E_{HF}^{\epsilon=\infty}$), and large interaction ($\Delta E_{HF}^{\epsilon=5}$). Such presentation of all the data on a single graph is justified by (i) the weak dependence of ΔE_{exp} on the twist angle near the magic angle (see Ref. [18] and Supplemental Material [20], Fig. S5) and (ii) the weak dependence of ΔE on θ_s if it is estimated as the spacing between the outermost singularities [Fig. 1(g)]. This is also why the Hartree-Fock model was calculated for a twist angle of 1.1° and $\theta_s = 30^\circ$. On the contrary, ΔE_{TB} were calculated with the full relative arrangement of the experimental data and show a better agreement with experiments. The twist angle has still a small influence, which explains the small deviations from a purely linear strain dependence. The measurements showing a cascade of transitions are indicated by a double border. (c) Relative deviation of ΔE_{exp}^0 to ΔE_{TB} as a function of the tunneling resistance $R_t = V_b/i_t$. The figure includes new unpublished data for the sample of Fig. 1(b) (red crosses).

tight-binding and the continuum model. On the contrary, the same data plotted as function of the twist angle do not show particular correlation with this parameter (Supplemental Material [20], Fig. S5).

Figure 2(c) provides a deeper level of comparison between theory and experiment. It presents the relative difference between the ΔE_{TB} and the experimental ΔE_{exp}^0 as function of the tunneling resistance $R_t = V_b/i_t$ (V_b and i_t are the tunneling bias and current). The deviations from the theory are small for $R_t > 2$ G Ω . They become larger at lower R_t , pointing to a possible influence of tip-induced strain which is known to be controlled by R_t [30]. The deformations seen in the additional measurements of Figs. 3(a)–3(c), showing of the evolution of the image of Fig. 1(b) for decreasing R_t , corroborate this interpretation

(the reader may also refer to Fig. S3 of Ref. [9] for another example).

Our measurements shown in Fig. 3 demonstrate that, while spatial variations of the LDOS at high R_t only reflect electronic localization in AA regions, the response to tip-induced strain at low R_t strongly depends on the position on the moiré pattern. While AB regions are weakly affected [Fig. 3(e)], ΔE_{exp} is reduced by 40% at low tunnel resistance in AA regions indicating a flattening of the bands [Fig. 3(d)]. The flattening culminates in intermediate regions between two AA regions where a 15 meV wide single LDOS peak signals that very flat bands can be engineered there [Fig. 3(f)]. It is not surprising that these regions are the most sensitive to tip-induced strain, because they are characterized by an excess of elastic

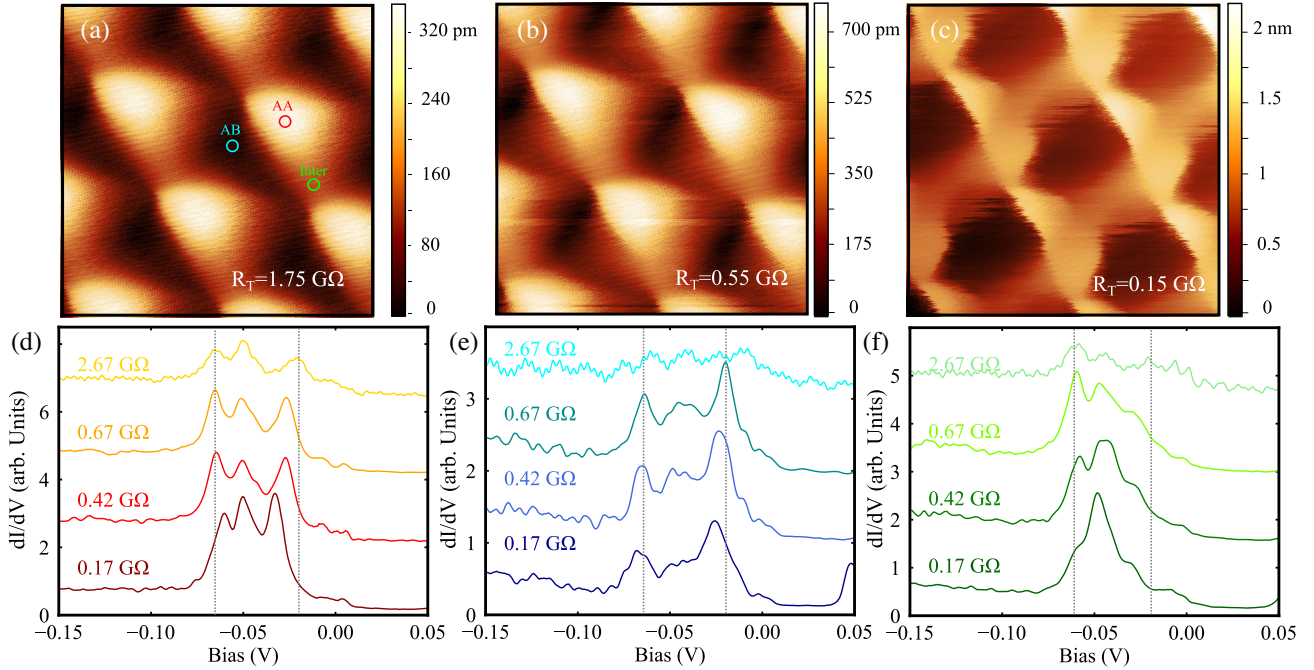


FIG. 3. Tip-induced strain. (a)–(c) STM images measured at decreasing tunneling resistance. The tunneling set point is $i_t = 100 \text{ pA}$ and the bias is (a) $V_b = 175$, (b) $V_b = 55$, and (c) $V_b = 15 \text{ mV}$. The images are $25 \times 25 \text{ nm}^2$. (d)–(f) Local density of states measured by STM for decreasing tunneling conductance in (d) AA, (e) AB, and (f) intermediate regions. The vertical dotted lines are guides for the eyes to track the position of the LDOS peaks. The tip-sample interaction was defined by the tunneling set point prior to switching off the feedback loop and subsequent sweeping of the bias voltage between -200 and 200 mV . In each panel from top to bottom, the tunneling set point is $i_t = 100 \text{ pA}$ and the bias is, respectively, $V_b = -800$, $V_b = -200$, $V_b = -125$, and $V_b = -50 \text{ mV}$. The dI/dV (V) signal was measured using phase sensitive detection with a 2 mV oscillation at 263 Hz added to the tunnel bias. The dI/dV curves were normalized to 1 at -200 mV .

energy [31–34] and are therefore more easily perturbed. We note that the tip may induce a complex strain pattern including hetero- or homostain, as well as vertical displacement, all of which depend on the position on the moiré. It follows that the relative arrangement between the layers can no longer be determined from STM images at low R_t , and that the response to tip-induced strain is largely sample dependent. This is illustrated by Fig. S5 of Ref. [9] in which, contrary to our experiment, the spacing between van Hove singularities increases with decreasing R_t . We therefore prescribe to perform the spectroscopic measurements at the highest possible tunneling resistance and to pay great care to the quantitative discussion of experimental results. From this perspective, Fig. 2(c) shows that the data used to construct Fig. 2(b) do not deviate from theory by more than 20%. It follows that Fig. 2(c) can be considered, to a large extent, as free of tip-induced strain effects. Also, from the large deviations that we could intentionally achieve in our sample [see red crosses in Fig. 2(c) and data in Fig. 3], we conclude that the STM tip can be used to locally engineer the relative arrangement between the layers.

The very good agreement between experiments and theory obtained so far raises the question about the influence of heterostrain on electronic correlations which role is more

important at zero doping [8–13]. Figure 2(b) shows that ΔE_{exp}^* , the experimental spacing of van Hove singularities in this regime, is increased by electronic correlations and increases with strain. This tendency is well pictured by our Hartree-Fock calculations presented in Fig. 2(b), including both heterostrain and electron-electron interactions for the dielectric constant $\epsilon = 5$ (see Refs. [20,35]). These calculations, however, underestimate ΔE_{exp}^* . Further increasing the effect of interactions by decreasing the dielectric constant does not lead to a better agreement, especially at large strains where the low-energy bands become so wide that they merge into the continuum of the higher energy bands and van Hove singularities can no longer be clearly defined [20]. Also, the calculations do not capture the large experimental scatter of ΔE_{exp}^* , which we were not able to correlate to any experimental parameter (twist angle, heterostrain value, or angle of application, bandwidths as measured by the FWHM of van Hove singularities, tunneling resistance, temperature). The scatter also does not correlate with the appearance of polarized states, leading to the cascade of transitions seen in some samples at intermediate fillings [13–15]. This points to a strong sensitivity of electronic correlations to some additional experimental parameters beyond those investigated

here. This could be due to the substrate or, more generally, to the detailed electrostatic environment, as suggested by several studies reviewed in Ref. [36], and to atomic lattice relaxation effects [33], calling for a systematic experimental study of the effect of those parameters.

Returning to heterostrain, its strong impact on the flat bands of magic-angle twisted graphene layers also calls for a systematic investigation of its influence on the strongly correlated phases and that of other moiré materials. In this context, it would be extremely desirable to be able to tune it. Alternatively, one could also rely of the variability in the fabrication process to generate a representative set of samples such as the one we have studied here.

The authors thank E. Andrei and S. Nadj-Perge for sharing their data and for interesting discussions. A. M. is supported by Paris-Seine Excellence Initiative (Grant No. 2019-055-C01-A0). F.G. and T.C. acknowledge funding from the European Commission, under the Graphene Flagship, Core 3, Grant No. 881603, and from Grants No. NMAT2D (Comunidad de Madrid, Spain), No. SprQuMat, and No. SEV-2016-0686 (Ministerio de Ciencia e Innovación, Spain).

*florie.mesple@cea.fr

†vincent.renard@cea.fr

- [1] Y. Cao *et al.*, Unconventional superconductivity in magic-angle graphene superlattices, *Nature (London)* **556**, 43 (2019).
- [2] Y. Cao *et al.*, Correlated insulator behaviour at half-filling in magic-angle graphene superlattices, *Nature (London)* **556**, 80 (2018).
- [3] G. Trambly de Laissardière, D. Mayou, and L. Magaud, Localization of Dirac electrons in rotated graphene bilayers, *Nano Lett.* **10**, 804 (2010).
- [4] R. Bistritzer and A. H. MacDonald, Moiré bands in twisted double-layer graphene, *Proc. Natl. Acad. Sci. U.S.A.* **108**, 12233 (2011).
- [5] S. Carr, S. Fang, P. Jarillo-Herrero, and E. Kaxiras, Pressure dependence of the magic twist angle in graphene superlattices, *Phys. Rev. B* **98**, 085144 (2018).
- [6] M. Yankowitz, S. Chen, and C.R. Dean, Tuning superconductivity in twisted bilayer graphene, *Science* **363**, 1059 (2019).
- [7] L. Huder, A. Artaud, T. Le Quang, G. Trambly de Laissardière, A. G. M. Jansen, G. Lapertot, C. Chapelier, and V. T. Renard, Electronic Spectrum of Twisted Graphene Layers under Heterostrain, *Phys. Rev. Lett.* **120**, 156405 (2018).
- [8] A. Kerelsky *et al.*, Maximized electron interactions at the magic angle in twisted bilayer graphene, *Nature (London)* **572**, 95 (2019).
- [9] Y. Choi *et al.*, Electronic correlations in twisted bilayer graphene near the magic angle, *Nat. Phys.* **15**, 1174 (2019).
- [10] Y. Jiang, X. Lai, K. Watanabe, T. Taniguchi, K. Haule, J. Mao, and E. Y. Andrei, Charge order and broken rotational symmetry in magic-angle twisted bilayer graphene, *Nature (London)* **573**, 91 (2019).
- [11] Y. Xie, B. Lian, B. Jäck, X. Liu, C.-L. Chiu, K. Watanabe, T. Taniguchi, B. Andrei Bernevig, and A. Yazdani, Spectroscopic signatures of many-body correlations in magic-angle twisted bilayer graphene, *Nature (London)* **572**, 101 (2019).
- [12] Z. Zhang, R. Myers, K. Watanabe, T. Taniguchi, and B. J. LeRoy, Probing the wave functions of correlated states in magic angle graphene, *Phys. Rev. Research* **2**, 033181 (2020).
- [13] D. Wong, K. P. Nuckolls, M. Oh, B. Lian, Y. Xie, S. Jeon, K. Watanabe, T. Taniguchi, B. Andrei Bernevig, and A. Yazdani, Cascade of electronic transitions in magic-angle twisted bilayer graphene, *Nature (London)* **582**, 198 (2020).
- [14] Y. Choi *et al.*, Correlation-driven topological phases in magic-angle twisted bilayer graphene, *Nature (London)* **589**, 536 (2021).
- [15] K. P. Nuckolls, M. Oh, D. Wong, B. Lian, K. Watanabe, T. Taniguchi, B. Andrei Bernevig, and A. Yazdani, Strongly correlated Chern insulators in magic-angle twisted bilayer graphene, *Nature (London)* **588**, 610 (2020).
- [16] Y. Zhang, Z. Hou, Y.-X. Zhao, Z.-H. Guo, Y.-W. Liu, S.-Y. Li, Y.-N. Ren, Q.-F. Sun, and L. He, Electron interactions in strain-induced zero-energy flat band in twisted bilayer graphene near the magic angle, [arXiv:2002.10073](https://arxiv.org/abs/2002.10073).
- [17] D. A. Cosma, J. R. Wallbank, V. Cheianov, and V. I. Fal, Moiré pattern as a magnifying glass for strain and dislocations in van der Waals heterostructures, *Faraday Discuss.* **173**, 137 (2014).
- [18] Z. Bi, N. F. Q. Yuan, and L. Fu, Designing flat bands by strain, *Phys. Rev. B* **100**, 035448 (2019).
- [19] X. Lu *et al.*, Superconductors, orbital magnets and correlated states in magic-angle bilayer graphene, *Nature (London)* **574**, 653 (2019).
- [20] See Supplemental Material at <http://link.aps.org/supplemental/10.1103/PhysRevLett.127.126405> for theoretical details and additional results, which includes Refs. [21–26].
- [21] J. M. B. Lopes dos Santos, N. M. R. Peres, and A. H. Castro Neto, Graphene Bilayer with a Twist: Electronic Structure, *Phys. Rev. Lett.* **99**, 256802 (2007).
- [22] H. Suzuura and T. Ando, Phonons and electron-phonon scattering in carbon nanotubes, *Phys. Rev. B* **65**, 235412 (2002).
- [23] V. M. Pereira and A. H. Castro Neto, Strain Engineering of Graphene's Electronic Structure, *Phys. Rev. Lett.* **103**, 046801 (2009).
- [24] F. Guinea, M. I. Katsnelson, and A. K. Geim, Energy gaps and a zero-field quantum Hall effect in graphene by strain engineering, *Nat. Phys.* **6**, 30 (2010).
- [25] N. N. T. Nam and M. Koshino, Lattice relaxation and energy band modulation in twisted bilayer graphene, *Phys. Rev. B* **96**, 075311 (2017).
- [26] T. Cea and F. Guinea, Band structure and insulating states driven by Coulomb interaction in twisted bilayer graphene, *Phys. Rev. B* **102**, 045107 (2020).
- [27] A. Artaud, L. Magaud, T. Le Quang, V. Guisset, P. David, C. Chapelier, and J. Coraux, Universal classification of twisted, strained and sheared graphene moiré superlattices, *Sci. Rep.* **6**, 25670 (2016).

- [28] I. Brihuega, P. Mallet, H. González-Herrero, G. Trambly de Laissardière, M.M. Ugeda, L. Magaud, J.M. Gómez-Rodríguez, F. Ynduráin, and J.-Y. Veuillen, Unraveling the Intrinsic and Robust Nature of van Hove Singularities in Twisted Bilayer Graphene by Scanning Tunneling Microscopy and Theoretical Analysis, *Phys. Rev. Lett.* **109**, 196802 (2012).
- [29] G. Trambly de Laissardière, D. Mayou, and L. Magaud, Numerical studies of confined states in rotated bilayers of graphene, *Phys. Rev. B* **86**, 125413 (2012).
- [30] H. J. Mamin, E. Ganz, D. W. Abraham, R. E. Thomson, and J. Clarke, Contamination-mediated deformation of graphite by the scanning tunneling microscope, *Phys. Rev. B* **34**, 9015 (1986).
- [31] J. S. Alden, A. W. Tsen, P. Y. Huang, R. Hovden, L. Brown, J. Park, D. A. Muller, and P. L. McEuen, Strain solitons and topological defects in bilayer graphene, *Proc. Natl. Acad. Sci. U.S.A.* **110**, 11256 (2013).
- [32] M. M. van Wijk, A. Schuring, M. I. Katsnelson, and A. Fasolino, Relaxation of moiré patterns for slightly misaligned identical lattices: Graphene on graphite, *2D Mater.* **2**, 034010 (2015).
- [33] H. Yoo *et al.*, Atomic and electronic reconstruction at the van der Waals interface in twisted bilayer graphene, *Nat. Mater.* **18**, 448 (2019).
- [34] Y. N. Gornostyrev and M. I. Katsnelson, Origin of the vortex displacement field in twisted bilayer graphene, *Phys. Rev. B* **102**, 085428 (2020).
- [35] T. Cea, N. R. Walet, and F. Guinea, Electronic band structure and pinning of Fermi energy to van Hove singularities in twisted bilayer graphene: A self-consistent approach, *Phys. Rev. B* **100**, 205113 (2019).
- [36] L. Balents, C. R. Dean, D. K. Efetov, and A. F. Young, Superconductivity and strong correlations in moiré flat bands, *Nat. Phys.* **16**, 725 (2020).